SCIENTIFIC REPORTS

OPEN

Hierarchical Flowerlike 3D nanostructure of Co$_3$O$_4$@MnO$_2$/N-doped Graphene oxide (NGO) hybrid composite for a high-performance supercapacitor

Sivalingam Ramesh[1], K. Karuppasamy [2], Hyun-Seok Kim[2], Heung Soo Kim[1] & Joo-Hyung Kim[3]

The present study investigates the fabrication of hierarchical 3D nanostructures with multi-component metal oxides in the presence of highly-porous graphene and characterized for its applications in high-performance supercapacitors. A hierarchical flowers like 3D nanostructure of Co$_3$O$_4$ @MnO$_2$ on nitrogen-doped graphene oxide (NGO) hybrid composite was synthesized by thermal reduction process at 650 °C in the presence of ammonia and urea. The synthesized Co$_3$O$_4$@MnO$_2$/NGO hybrid composites were studied *via* Raman, XRD, X-ray XPS, FE-SEM, FE-SEM with EDX, FE-TEM and BET analyses. The electrochemical analysis of Co$_3$O$_4$@MnO$_2$/NGO hybrid composite electrode was investigated using cyclic voltammetry, chronopotentiometry and electrochemical impedance measurements. The hybrid composite electrode showed significant specific capacitance results of up to 347 F/g at 0.5 A/g and a corresponding energy density of 34.83 Wh kg^{-1} with better rate performance and excellent long-term cycling stability were achieved for 10,000 cycles. The obtained electrochemical results paved a way to utilize Co$_3$O$_4$@MnO$_2$/NGO composite electrode as a promising electrode material in high performance supercapacitors.

Supercapacitors have received a great deal of consideration since they can comprise renewable energy storage devices with improved power density, cycling stability, low cost, and wide operating temperature ranges. In general, the carbon materials, metal oxides, metal hydroxides and conducting polymers are extensively employed as active materials for energy storage applications. Based on the electrochemical behaviors, the metal oxides have a high specific capacitance due to redox behaviors in the electrode materials. But, unfortunately, some of the metal hydroxides investigated earlier possess poor electrical conductivity that hinders the capacitive behavior[1–4]. In order to overcome the low capacitance behaviors, researchers have aimed to improve the electrical conductivity of the metal oxide with carbon materials for high-performance supercapacitors[5–7]. These hybrid composites have synergetic properties due to a combination of metal oxide or hydroxides in the presence of a redox reaction.

Recently, derivatives of graphene which include graphene oxide (GO), reduced graphene oxide (rGO) and N-doped GO have been utilized extensively for supercapacitor applications. These oxide functional moieties of graphene oxide interact with metal oxides to form M-O-M bonds which in turn facilitates the ionic mobility and diffusion rate and improves the performance of electrochemical double-layer capacitance (EDLC)[5–7]. Furthermore, the graphene and graphene oxides are chemically modified to improve the electrochemical performances[8–10]. The efficient chemical route is to dope the graphene with heteroatoms, such as nitrogen (N) and sulfur can be enhanced the electron mobility and capacitance in presence of valence electrons. Therefore, the NGO has attracted a significant amount of attention to synthesize the various chemical processes such as CVD and hydrothermal reactions.

[1]Department of Mechanical, Robotics and Energy Engineering, Dongguk University–Seoul, Pildong-ro 1 gil, Jung-gu, Seoul, 04620, South Korea. [2]Division of Electronics and Electrical Engineering, Dongguk University–Seoul, Pildong-ro 1 gil, Jung-gu, Seoul, 04620, South Korea. [3]Department of Mechanical Engineering, Inha University, Inha-ro 100, Nam-gu, Incheon, 22212, South Korea. Correspondence and requests for materials should be addressed to Heung Soo Kim (email: heungsoo@dgu.edu) or J.-H.K. (email: joohyung_kim@inha.ac.kr)
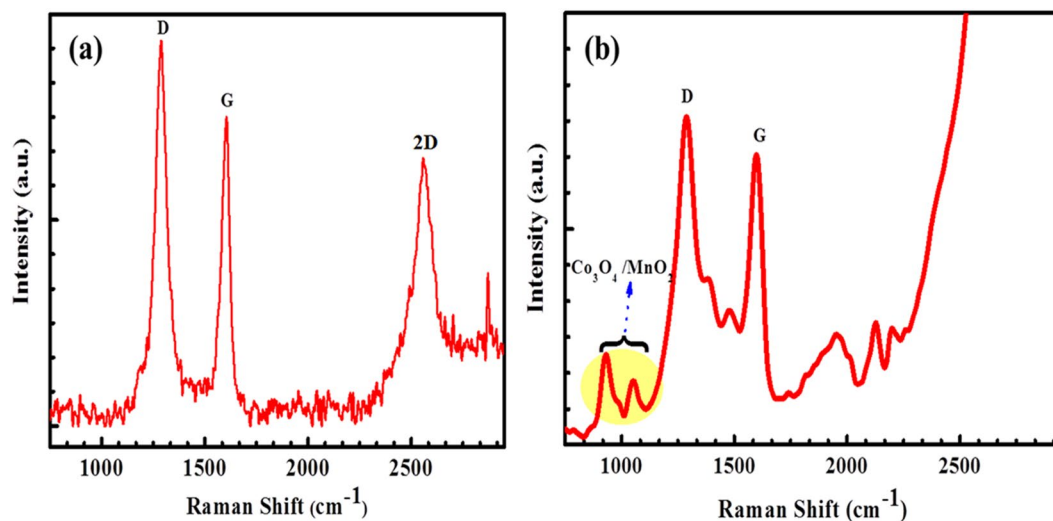
Figure 1. FT-Raman analysis of (**a**) NGO and (**b**) Co_3O_4@MnO_2/NGO composite electrode.

Zhu *et al*. reported on CVD-derived NGO sheets by organic molecules *via* carbon and nitrogen atoms doped with higher concentration and growth temperature[11]. In addition, the carbon-based materials with a porous structure, transition-metal oxides and conjugated polymers are important active electrode materials for supercapacitors[12–14]. Transition metal oxides such as nickel (Ni), cobalt (Co), and manganese (Mn) oxides offer superior physiochemical properties and comprise excellent electrochemical supercapacitors[15]. In particular, cobalt oxide (Co_3O_4) is considered to be an auspicious electrode material for supercapacitors because of its economically cheap, high redox activity, high surface area and easily tunable surface properties. The nanostructured Co_3O_4 is the most stable cobalt oxide with a spinel structure and important p-type semiconductor which is widely used in Li-ion batteries, heterogeneous catalysts, electrochemical capacitors, electrochromic devices, solid-state sensors, solar selective absorbers for high-performance supercapacitors[15–17]. The hierarchical 3D structure provides a high surface area and rapid electron transport from the electroactive materials to the current collector, which may be due to the active material being grown directly on the current collector and avoiding the binders that normally cause a decrease in the electrode conductivity[17–21].

Various types of MnO_2, MnO_2/graphene, MnO_2/Zn_2SnO_4, MnO_2/Cu, and MnO_2/conducting polymers were used for supercapacitors applications[22–31]. Furthermore, the binary and ternary nanostructures of the hybrid composites are promising materials including Co_3O_4@MnO_2, NiO/Ni core−shell, $Ni(OH)_2$−MnO_2/GO that have been widely used as electrodes for supercapacitors[32–35]. Therefore, the electrochemical properties of the nanostructured materials show a strong effect on the morphology to increase the specific capacitance and electro-catalysis towards capacitors, oxygen evolution (ORR) and (OER) reactions[36,37].

Herein we report a hierarchical flower like 3D nanostructured Co_3O_4@MnO_2/NGO composite electrodes for electrochemical supercapacitor for the first time. The prepared Co_3O_4@MnO_2/NGO and aqueous 6 M KOH solution have been utilized as working electrode and electrolyte respectively to evaluate the capacitive performance of the cell. Furthermore, the physicochemical properties of the Co_3O_4@MnO_2/NGO electrode have been determined through Raman, XRD, XPS, FE-SEM, EDX, BET and FE–TEM analyses. The salient features of the present electrode system are discussed herein.

Results and Discussions

The GO exhibits a considerable increase in the intensity ratio between D and G peaks have been evidenced through Raman analysis. In previous reports, the GO materials showed remarkable peaks at 1340 and 1590 cm^{-1}, indicates that the D-band arises from the edge or defect sites of carbon and G band indicating the *sp^2* carbon of the graphene sheets[38]. The Raman spectra of the Co_3O_4@MnO_2/NGO hybrid composite materials obtained *via* hydrothermal processing are shown in Fig. 1. The GO in the Co_3O_4@MnO_2/NGO electrode structure is confirmed by the appearance of dominant peaks at 1345 cm^{-1} and 1589 cm^{-1} represents the D and G bands correspondingly. The D and G bands are meant for disordered *sp^3* carbon and well-ordered in-plane sp^2 carbon bonds respectively which are in great resemblance with our recent reported result on MWCNT/GO/$NiCo_2O_4$ hybrid electrodes[38]. Further, the acquired results are in greatly concurrent with other previous reported literatures on graphene based composite materials[39,40].

The XRD analysis of graphite, graphene oxide, reduced and nitrogen graphene oxides were previously reported in the literature[40]. The graphite powder showed characteristic diffraction peak at 2θ = 26.50°, and the corresponding layer-to-layer distance was ~0.36 nm. After the oxidation of graphite powder to GO in the presence of $KMnO_4$, the diffraction peak shifted towards left at angle of 2θ = 10.40°, and the layer distance of ~0.89 nm confirmed the GO structure. In addition, the diffraction peak shown at around 2θ = 43° represents the graphene oxide with a turbostratic disorder behaviours[41–43]. In the present study, the results for the Co_3O_4@MnO_2/NGO hybrid composite are shown in Fig. 2(a,b). It is observed from the Fig. 2(a,b) that the XRD patterns of Co_3O_4/NGO and Co_3O_4@MnO_2/NGO hybrid composites consists of clearly distinguished peaks and the corresponding
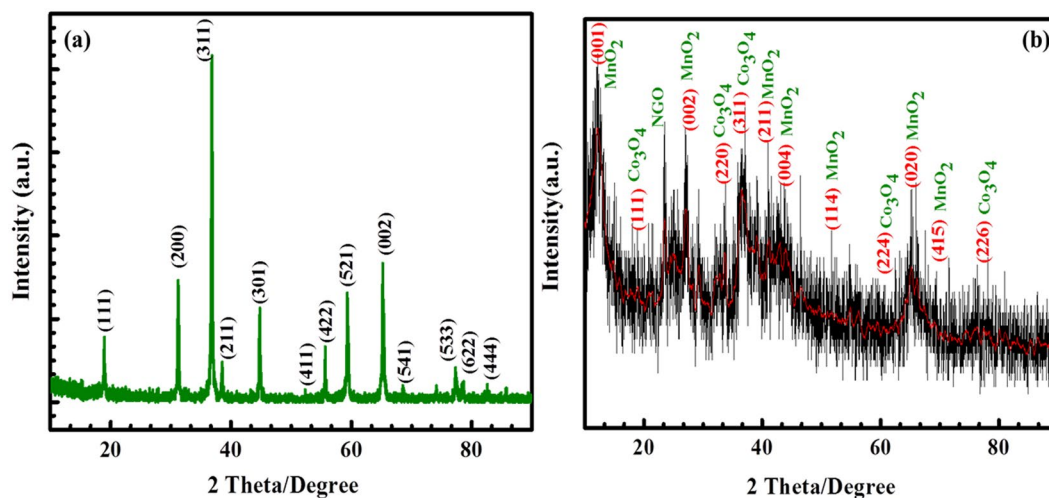
Figure 2. XRD results of (**a**) NGO/Co_3O_4 and (**b**) Co_3O_4@MnO_2/NGO hybrid composites.

planes exactly matches well with the JCPDS PDF file data [42–1467]. The peaks at 18.96°, 31.20°, 36.74°, 38.28°, 44.72°, 55.44°, 59.20°, 65.10°, 77.12°, and 82.27° corresponds to (111), (22 0), (311), (222), (4 00), (422), (511), (44 0), (533), and (622) reflection planes of Co_3O_4/GO and pure Co_3O_4. The pattern resembles with the spinel Co_3O_4 structure and matches well with the Joint Committee on Powder Diffraction Standards (JCPDS) card [42–1467]. In addition, the analysis confirms that the crystal structure of the Co_3O_4 was maintained during the formation of the MnO_2 on the Co_3O_4 nanoparticles in the core shell-like structure. The MnO_2 nanoparticles are arranged in birnessite δ-MnO_2 with broad and weak peaks at 12.52° (001), 25.26° (002), 36.20° (111), and 65.64° (020) due to the formation of Co_3O_4@MnO_2 core-shell nanoparticles in the hybrid composite with good agreement of the birnessite-MnO_2 (JCPDS No. 80–1098). The broad graphitic (002) and weak (100) peaks are proven as GO materials, and the disorderedly stacked GO sheets in the hybrid composite[44,45].

The elements and chemical states of the Co_3O_4@MnO_2/NGO composite have been studied through XPS analysis and the resultant results are depicted in Fig. 3. As shown in Fig. 3, the Mn 2p, Co 2p, C 1s, O 1s and N 1s are found with their corresponding binding energies (BE). In addition, the XPS spectrum of C 1s peaks corresponds to C 1s (284–295 eV), O 1s (529.6 eV), O* 1s (532 eV) from Mn and Co oxides, N 1s (398–406.9 eV) present in the hybrid composite. Therefore, the nitrogen (N 1s) spectrum can usually be deconvoluted into three individual peaks, namely pyridine nitrogen (N), pyrrolic nitrogen (N) and graphite nitrogen (N), as confirmed in the hybrid composite. Besides the O 1s peak and Co 2s peak, two distinct peaks located at binding energies of 642.0 and 653.1 eV were observed in the Mn 2p core level spectrum, indicates that the Mn $2p_{3/2}$ and Mn $2p_{1/2}$ in manganese oxide present in the hybrid composite. The peak values are in concurrent with the earlier report of MnO_2, indicating a +4 oxidation state of Mn[46]. These results provide direct evidence of Co_3O_4@MnO_2 core shell nanoparticles in the hybrid composite obtained via thermal reduction process.

The surface morphology of the prepared Co_3O_4@MnO_2/NGO electrode has evidenced through SEM analysis. The SEM images at different magnifications of Co_3O_4@MnO_2/NGO are shown in Fig. 4(a–e). Its corresponding EDX spectrum is provided in Fig. 4(f). As it can be seen that the compact Co_3O_4@MnO_2/NGO sheets grew vertically on the surface and assembly of these sheets in turn form a hierarchical porous structure as shown in Fig. 4(a–e). The obtained results strongly supports the results obtained from HR-TEM analysis which will be discussed further in the later section.

Figure 5(a–g) shows the HR-TEM morphology and Fig. 5(h,i) the SAED patterns of Co_3O_4@MnO_2/NGO hybrid nanocomposite.

The Co_3O_4@MnO_2 electrode possess hierarchical flower-like morphology as represented Fig. 5 with the particle size in the range between 10 and 20 nm and decorated homogeneously over the NGO surface. The SAED patterns in Fig. 5(h,i) specify an ordered rings, which is owe to be the hierarchical flower like structure of Co_3O_4@MnO_2.

Based on the pore structure, the active electrode surface of the porous carbon electrode for EDLCs is highly useful for supercapacitors in the presence of various electrolytes. Therefore, the porous structure of the porous carbon materials influences the energy/power densities in the electrochemical properties. Cobalt (Co) and manganese (Mn) electrodes are highly desirable for supercapacitor or batteries applications with enhanced surface properties[47]. The BET results of Co_3O_4@MnO_2/NGO at 77 K are displayed in Fig. 6.

The N_2 adsorption-desorption isotherm characteristics of the Co_3O_4@MnO_2/NGO hybrid composite shows type II hysteresis loop as shown in Fig. 6(a). The surface area, pore volume, pore area and pore diameter values are ~350 m²/g, 0.55 cm³/g, 44 m²/g and 60 A° respectively. Furthermore, the surface area of Co_3O_4@MnO_2/NGO increases, and the electrochemical behavior, such as the specific capacitance and cyclic stability, increases when compared to previously-reported hybrid composites[48–50].

The electrochemical properties of various nanostructured carbon-based Co_3O_4, MnO_2, Co_3O_4@MnO_2 core/ shell and its electrochemical properties were previously reported in the literature[48–50]. This cobalt (Co_3O_4) and
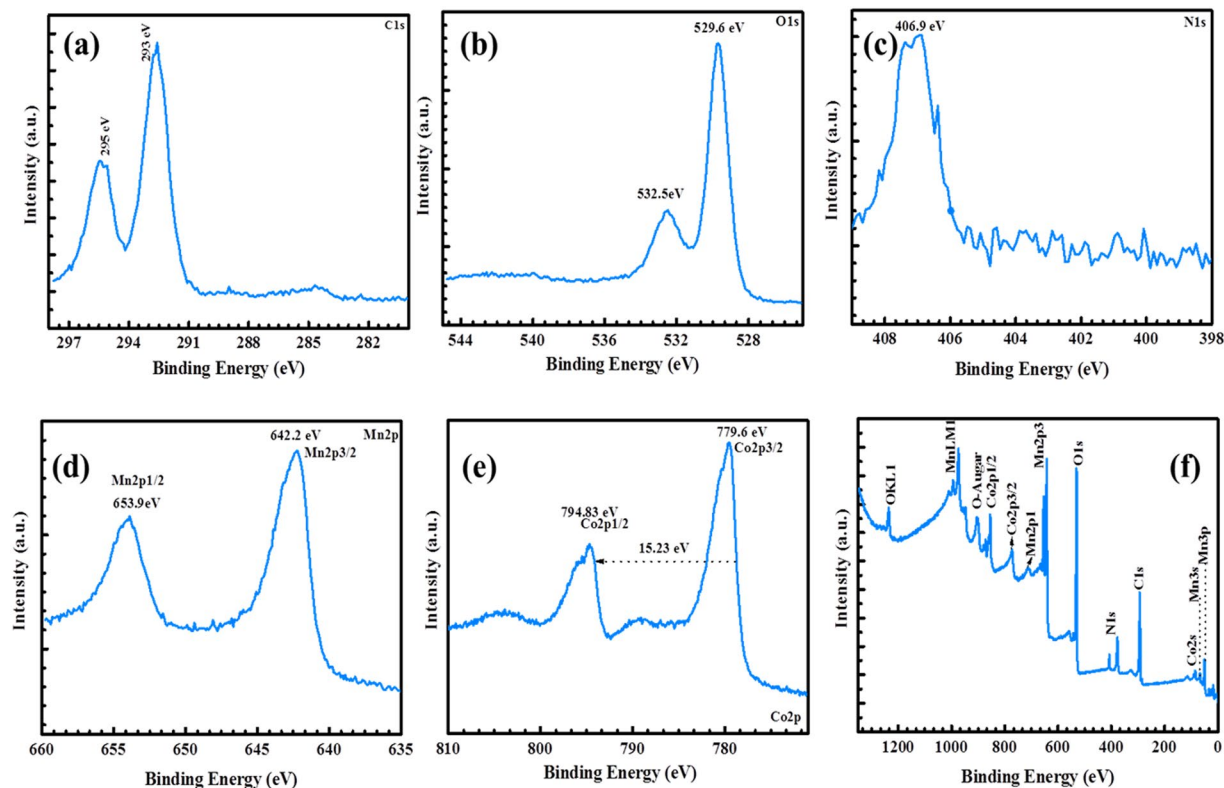
Figure 3. XPS results (**a**) C1s (**b**) O1s (**c**) N1s (**d**) Mn 2p (**e**) Co2p energy levels of hybrid composite.

MnO_2 materials clearly shows the redox behaviors of the metal oxide and different oxidation states (Co^{3+}/Co^{4+}) in the presence of a strong electrolyte *via* electrochemical reactions. Based on previous reports, the electrochemical properties of the $Co_3O_4@MnO_2/NGO$ hybrid composite have been investigated in a three-electrode configuration for CV, GCD and EIS experiments. The typical three-electrode cell containing $Co_3O_4@MnO_2/NGO$ ternary hybrid composite, Ag/AgCl, and Pt electrodes as working, reference, and counter electrodes, respectively, was dipped in 6 M aqueous KOH solution at room temperature. These results of the as-prepared $Co_3O_4@MnO_2/NGO$ electrodes in the different scans rates from (10 to 100 ms/V) are shown in Fig. 7. The CV curves are almost similar at all scan rates, indicating the reversible nature of the hybrid composite electrodes. The shape of the CV peaks represents the charge-discharge mechanism of the $Co_3O_4@MnO_2/NGO$ hybrid electrode via faradic reaction (oxidation and reduction reaction) of the metal ions together with 6 M KOH to improve the rate of reaction. Therefore, the CV area represents the total charge accumulating through the Faradaic and non-Faradic reaction. The faradaic contribution involves ion migrations with a surface-bound redox capacitance, whereas the non-Faradaic process is and effect of the double layer capacitance. The electrochemical properties of GO, RGO, NGO, Co_3O_4, MnO_2 and $Co_3O_4@MnO_2$ hybrid composites have been reported in the literature[51–53].

Figure 7 represents the CV results of the $Co_3O_4@MnO_2/NGO$ composite electrode. The results of the CV curves for all electrodes shows a symmetrical behavior of the ideal capacitive properties with a quasi-rectangular shape due to the excellent capacitive nature of the electrodes. A close observation of the CV results of the hybrid composite electrodes indicates a more rectangular behaviour and a relative increment in the current level compared to that of pristine cobalt and manganese oxide materials[51–53]. These properties of the hybrid composites show the overall specific capacitance due to the combined contribution from EDLC and the pseudo-capacitance behaviour, and its related reversible reaction of $Co_3O_4@MnO_2$ nanoparticles in the presence of a strong electrolyte. Based on the reversible reaction, the CV measurements have conducted at various scan rates, and the relative current response occurred with an ideal capacitive response of the $Co_3O_4@MnO_2/NGO$ composite.

It is perceived from the CV plot that the anodic and cathodic peaks are increases with increasing current density and sweep rates and the position of the peaks remains unaltered which indicates the ions are migrated in the both directions. Hence, the redox reactions are ensues at the electrode-electrolyte interfaces in presence of the strong electrolyte. These results show a rectangular behaviour with certain deviation due to the hydroxyl functional groups present in the NGO materials. Therefore, the CV results of the NGO materials are much larger then graphene-based materials[54,55], which indicates the greater electrochemical properties of NGO. The specific capacitance values are calculated from Eq. (1) and these values are compared with earlier reports which are due to the surface properties of the electrolyte solution which reduces the internal resistance R_i thereby increase the pseudo-capacitance nature of the electrode material[54,55]. The CV results of (Fig. 7(a)) indicate that various scan rate of (10, 20, 40, 60, 80 and 100) mV s^{-1}, around 95% of the initial capacitance has retained. These enhanced performances of the hybrid composite represent the following features in the electrochemical reaction. The first one is, the $Co_3O_4@MnO_2/NGO$ containing the more electroactive sites and exist as both double layer and
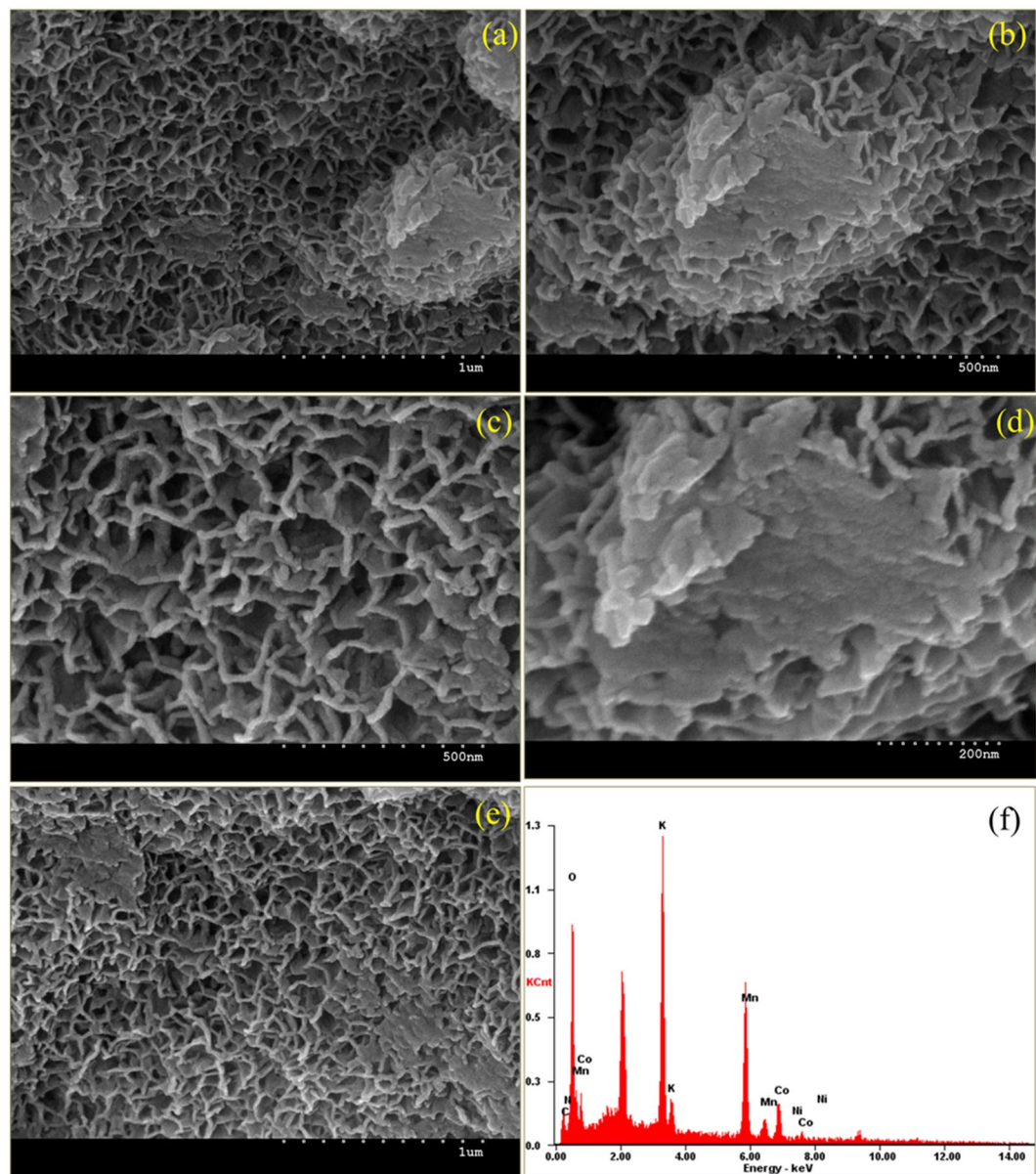
Figure 4. (**a**–**e**) FE-SEM morphology and (**f**) SEM-EDX of Co_3O_4@MnO_2/NGO hybrid composites.

pseudo-capacitance nature whereas the second one is due to decrement in internal resistance of the electroactive materials for enhancement of electrical conductivity[50–55].

Furthermore, the results of the galvanostatic charge-discharge (GCD) profile explained the practical applications of Co_3O_4@MnO_2/NGO hybrid composite. Figure 7(b–e) represents the GCD curves of the Co_3O_4@MnO_2/NGO electrode using 6 M KOH solution at different current densities under ambient temperature. The GCD from Fig. 7(b) demonstrates that it consists of triangular shape-voltage profile which confirms the existence of the EDLC and pseudo-capacitance nature and is in concurrent with the results obtained from CV analysis. The Co_3O_4@MnO_2/NGO electrodes offer the maximum discharge time than that of the pristine cobalt and manganese composites[30–37,56], which indicate that the capacity has been stored for a prolong time by the prepared Co_3O_4@MnO_2/NGO electrodes. The specific capacitance is calculated from Eq. (2) and it shows values of 347 Fg^{-1}, 264, and 184 $F\,g^{-1}$ at 0.5, 1, and 2 $A\,g^{-1}$ respectively. The specific capacitance values of Co_3O_4@MnO_2/NGO are quite high as compared to pristine Co_3O_4 and MnO_2 composites which are because of its higher electrical conductivity, migration of ions in electrolyte solution, and electrical double layer charge storage capacity. The specific capacitance decreases with increase in current density in the order of (0.5, 1, and 2) $A\,g^{-1}$. In addition, the electrochemical capacitance values are given in the (Table 1) with those of previously reported Co_3O_4@MnO_2/NGO hybrid composites prepared from cobalt and manganese materials[46–55,57].

Figure 7(c,d) illustrates the relation between power density and energy density (P vs E plot) and the capacity retention curve of the Co_3O_4@MnO_2/NGO composite. The energy and power densities have been calculated from Eq. (3) and (4), and result is demonstrated in Fig. 7 (c,d) which indicates the long term cyclic stability of the active
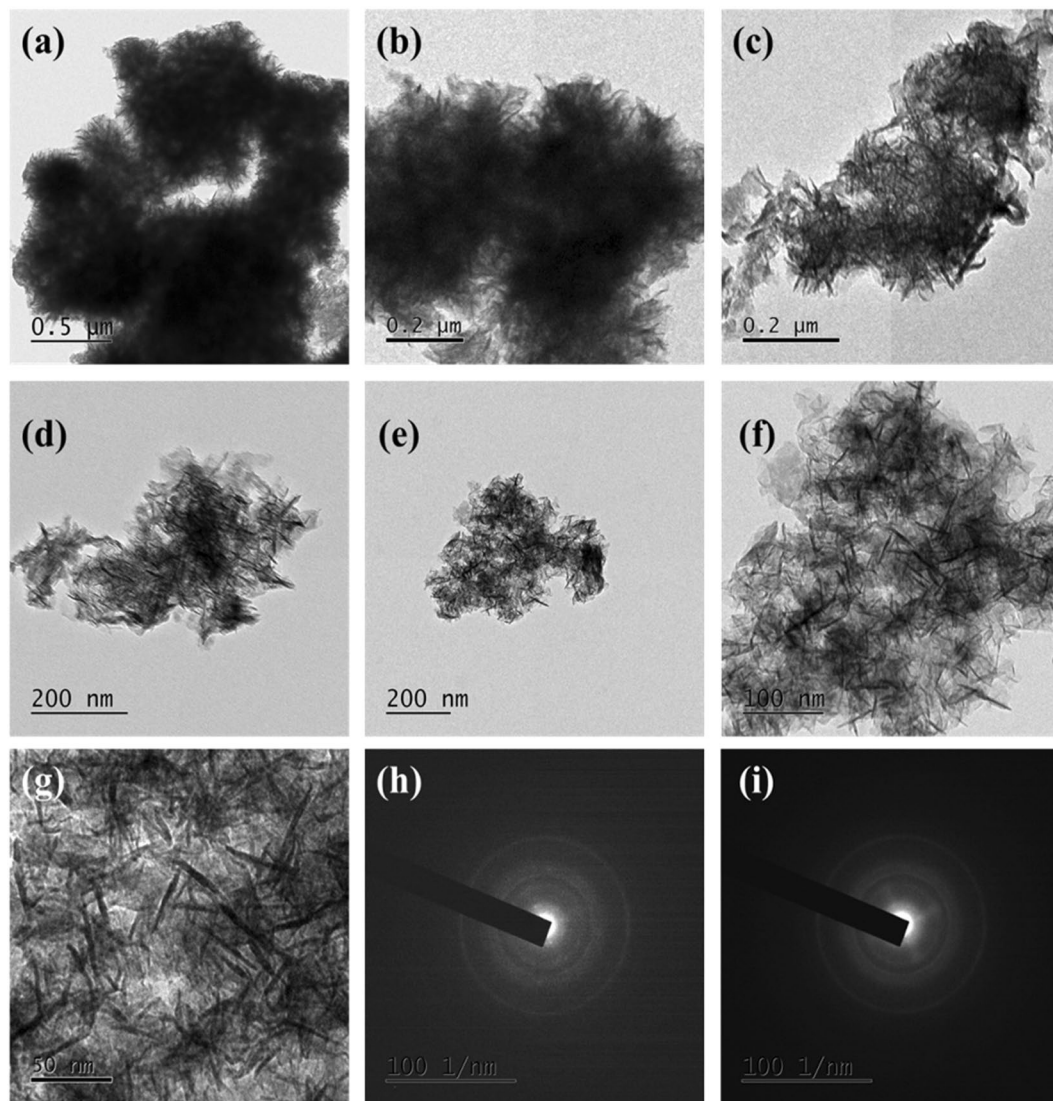
Figure 5. (**a**–**g**) FE-TEM images of $Co_3O_4@MnO_2/NGO$ at different particle sizes and (**h,i**) SAED array of $Co_3O_4@MnO_2/NGO$.
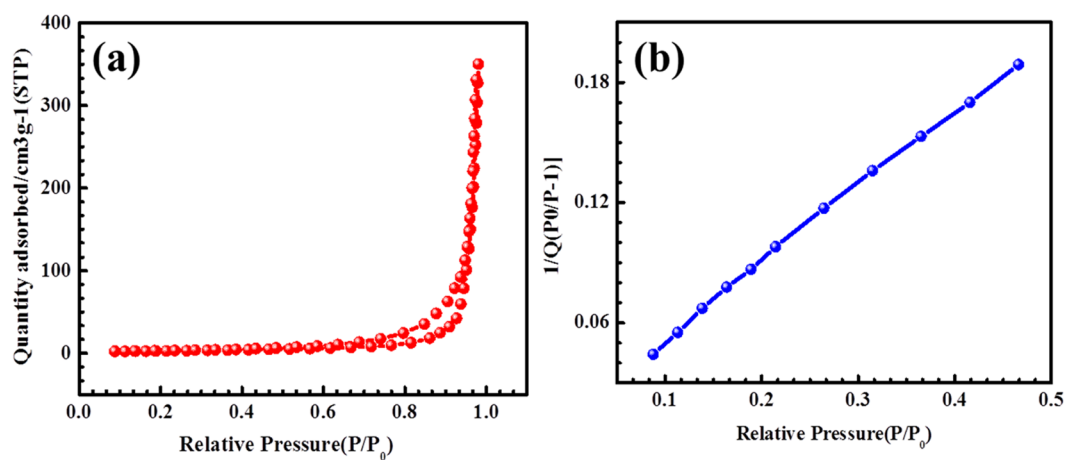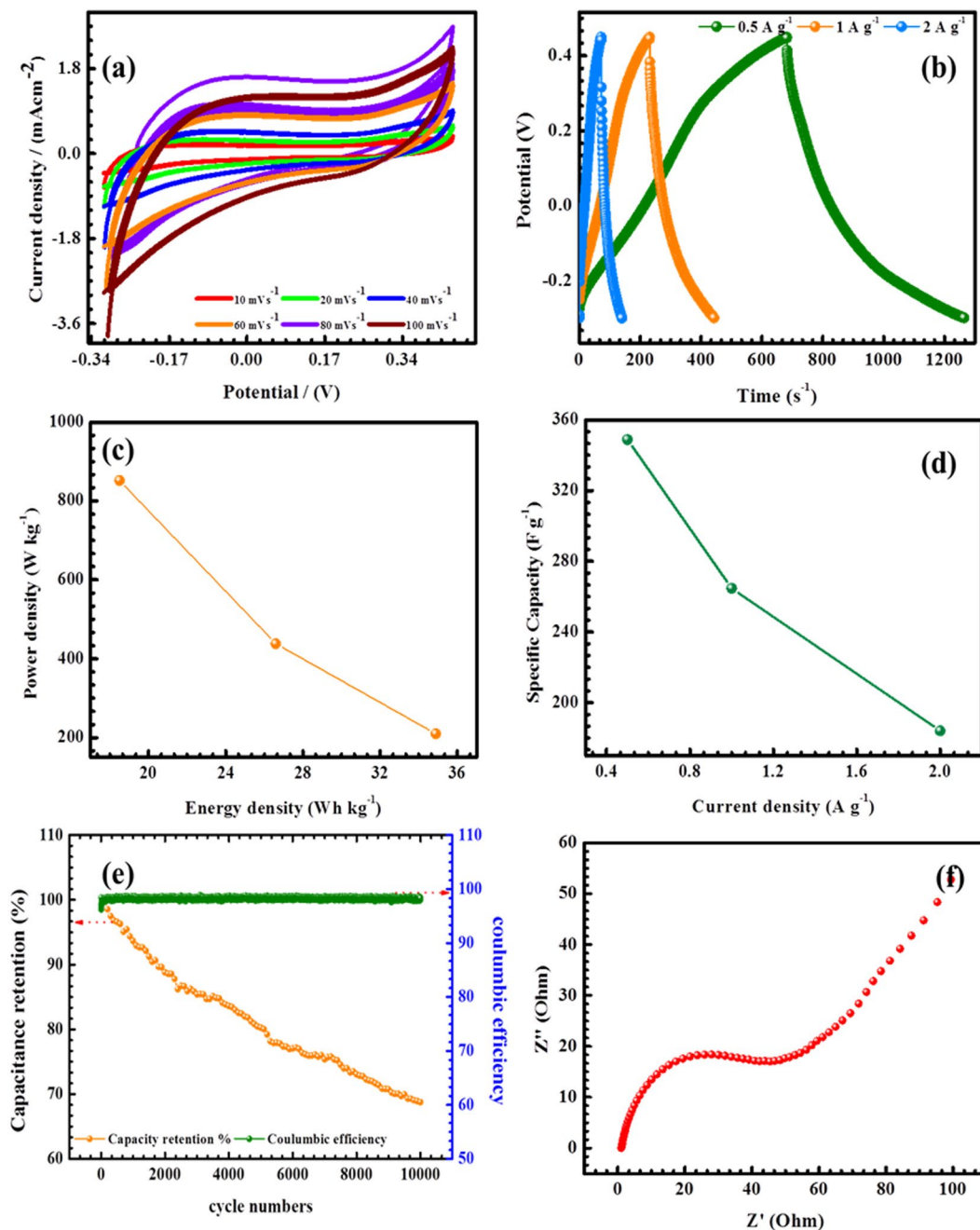

Figure 6. BET analysis of $Co_3O_4@MnO_2/NGO$ electrode.

Figure 7. (**a**) CV plots of the $Co_3O_4@MnO_2/NGO$ at different scan rates in the range between 10 to100 mV s^{-1}, (**b**) Galvanostatic charge-discharge behavior of the $Co_3O_4@MnO_2/NGO$ at various current densities, (**c**) Specific capacitance *vs* Current density plot, (**d**) Power density as function of energy density (**e**) Capacity retention plot for 10000 cycles (**f**) Nyquist impedance plot of the cell at ambient temperature.

electrode materials for supercapacitor applications. Further, the cyclic stability of the $Co_3O_4@MnO_2/NGO$ hybrid composite electrodes have been confirmed by repeating the GCD analysis at 0.5 A g^{-1} for 10,000 cycles and its corresponding plot and values are provided in Fig. 7(e) and Table 1 respectively. After 10,000 cycles, the $Co_3O_4@MnO_2/NGO$ reached 69% of its initial specific capacitance, which indicates that the electroactive material possess excellent cycling stability and reversibility[46–55,57]. Table 1 compares the electrochemical properties of the Co_3O_4, MnO_2 and $Co_3O_4@MnO_2$ electrodes with the $Co_3O_4@MnO_2/NGO$ hybrid composite.

In order to evaluate the internal resistance and capacitance of the prepared $Co_3O_4@MnO_2/NGO$ electrode, EIS have been performed in the frequency range between 0.1 Hz and 100 KHz. The results have analyzed by using Nyquist plots, which denotes the frequency reaction of the electrode/electrolyte. Figure 7(f) indicates the EIS results of $Co_3O_4@MnO_2/NGO$ electrode and its corresponding equivalent series resistance (ESR) has been evaluated from the intercept of the X-axis at high frequency which is the total combination of the ionic resistance of electrolyte, intrinsic resistance of composite electrode, and contact resistance at current collector interface. The

Electrode material	Preparation method	Capacitance (F g^{-1})	Cyclic stability	Ref
Porous Cobalt oxide nanocomposite	Hydrothermal process	226.3 F g^{-1} at 10 mVs^{-1}	24% loss after 5000 cycles	[46]
rGO/Cobalt oxide	Hydrothermal process	278.5 F g^{-1} at 200 m A g^{-1}	9.4% loss after 2000 cycles	[47]
Cauliflower like Co$_3$O$_4$	Hydrothermal process	863 F g^{-1} at 1 mVs^{-1}	No decay after 1000 cycles	[48]
Co$_3$O$_4$ decorated graphene	One –spot Solvothermal process	346 Fg^{-1} at 1 A g^{-1}	15% loss after 50 cycles	[49]
Co$_3$O$_4$@graphene	Hydrothermal synthesis	415 Fg^{-1} at 3 A g^{-1}	26% loss after 300 cycles	[50]
MnO$_2$/RGO composite	Electrochemical deposition	125.93 Fg^{-1} at 10 mV s^{-1}	20% loss after 5000 cycles	[51]
MnO$_2$ on graphene	Hydrothermal	280 Fg^{-1} at 1 A g^{-1}	9% loss after 10,000 cycles	[52]
Co$_3$O$_4$ nanotubes	Chemical deposition	273 Fg^{-1} at 0.5 A g^{-1}	22% loss after 500 cycles	[53]
Cobalt tungstate (CoWO$_4$)	Chemical precipitation reaction	1127.6 Fg^{-1} at 1 A g^{-1}	24.3% loss after 3,000 cycles	[54]
Co$_3$O$_4$@MnO$_2$ core shell nanostructure	hydrothermal approach	560 F g^{-1} at a current density of 0.2 A g^{-1}	5% loss after 5000cycles	[55]
Co$_3$O$_4$@pt@MnO$_2$	Nanowire arrays on the Ti substrate coating	497 F g^{-1} at 10 mV/s	No loss after 5000 cycles	[57]
Co$_3$O$_4$@MnO$_2$/NGO	**Thermal reduction process**	**347 F g^{-1} at 0.5 A g^{-1}**	**31% loss after 10,000 cycles**	**This work**

Table 1. Comparison of the supercapacitor values of various nanostructured of cobalt oxides (Co$_3$O$_4$), Manganese oxides (MnO$_2$) and Co$_3$O$_4$@MnO$_2$/NGO electrodes reported in the literature.

presence of straight line at lower frequency region and low ESR values may be due to the presence of Co$_3$O$_4$@MnO$_2$ in Co$_3$O$_4$@MnO$_2$/NGO electrode which enhanced the electrochemical properties of NGO. The value of ESR is ~40 Ω which indicates it has very small inherent resistance and the Warburg angle is higher than 45° at low frequencies which in turn due to the diffusion process at the electrode-electrolyte interfaces. Therefore, the charge transfer resistances of the electro active materials shows in lower frequency region were calculated 38–40 Ω respectively. The observed result strongly demonstrates the stable electrochemical properties of the Co$_3$O$_4$@MnO$_2$/NGO electrodes.

Conclusions

The controlled synthesis of hierarchal flower-like morphology of Co$_3$O$_4$@MnO$_2$/NGO hybrid composites have been synthesized *via* thermal reduction and investigated its electrochemical behavior for high-performance supercapacitors. The Co$_3$O$_4$@MnO$_2$/NGO composite electrode achieved the highest capacitance of 347 F g^{-1} at 0.5 A g^{-1}. The excellent electrochemical behavior of the Co$_3$O$_4$@MnO$_2$/NGO electrode was attributed to the high surface area and improved surface morphology, which facilitates the electron diffusion at the electrode/electrolyte interface. The long term cycling stability of the hybrid composite electrode was analyzed by subjecting the cell to GCD analysis at ambient conditions and it retained 69% of its capacitance after 10,000 charge–discharge cycles thereby demonstrating the excellent cyclic stability and reversibility of the prepared electrode material. The ESR and R$_{ct}$ values were lower for the Co$_3$O$_4$@MnO$_2$/NGO composite and hence it deeds as a promising candidate for high-performance supercapacitors.

Materials and Methods

The graphite powder was gifted from Alfa Aesar, South Korea and used as such. Sulfuric acid (H$_2$SO$_4$,), N-methyl-2-pyrrolidone (NMP), nitric Acid (HNO$_3$), polytetrafluorethylene (PTFE), potassium hydroxide (KOH), sodium nitrate (NaNO$_3$), hydrogen peroxide (H$_2$O$_2$), cobalt nitrate (Co(NO$_3$)$_2$.6H$_2$O), potassium permanganate (KMnO$_4$), and Manganese acetate (Mn(CH$_3$COO)$_2$.4H$_2$O) were used as the starting materials for cobalt and manganese oxides respectively. All the chemicals and solutions used in the present investigation were purchased from Sigma-Aldrich (South Korea).

Graphene oxide (GO) preparation process. The GO powder was made by modified Hummers procedure and reported elsewhere[58,59]. In brief, the stoichiometric amounts of graphite flakes (3 g) and H$_2$SO$_4$ (20 ml), NaNO$_3$ (1.4 g), were taken in a reaction flask and chilled to 0°C. Afterward, the KMnO$_4$ (0.18 g) was included in the reaction mixture slowly under room temperature. The resultant solution was subjected to stirring at 35°C for about 12 h and then 30% H$_2$O$_2$ was added into the reaction mixture followed by neutral pH. The resulting GO materials were washed with water and ethanol and subjected to vacuum at 40°C for 12 h. Finally, the finely dried GO powder was collected and kept in a desiccator.

Synthesis of nitrogen-doped graphene oxide (NGO). 1 g of GO was dispersed in 200 mL of H$_2$O under ultra-sonication treatment with high power pole for 4 h. The GO suspension thus obtained was filtered through Millipore (50 mm in diameter and 0.45 mm in pore size) filter and evaporated further at 95°C for duration of 12 h. The purified GO was dispersed in water and ammonia (10 ml)/urea (1 g) and it was continuously stirred for 12 h at 90°C. The resulted solution was dried at 180°C and then purified several times with water-ethanol mixture. Finally, the NGO powder was subjected to calcination at 200°C and it was collected for further characterization.

Synthesis of Co$_3$O$_4$@MnO$_2$/NGO hybrid composite. In a typical experiment, 0.3 g of NGO in 200 ml of water was stirred for about 2 h at 90°C. Then, the stoichiometric amounts of cobalt nitrate [Co(NO$_3$).6H$_2$O] (3 g), manganese acetate [Mn (CH$_3$COO)$_2$ 4H$_2$O] (1.5 g) and potassium permanganate (KMnO$_4$) (1.5 g), urea

(NH_2CONH_2) (1.2 g), and 30% aqueous ammonia solution were added and stirred continuously at 90 °C for 12 h. Initially, the solution was turbid due to the formation of cobalt /manganese hydroxides which was dissolved by adding excess ammonia/water. The transparent solution was then evaporated overnight at 90 °C under *vacuum*. The resulting product was purified using ethanol/water and calcined at 650 °C for 8 h *via* thermal reduction process.

Materials Characterization.

The NGO and $Co_3O_4@MnO_2$/NGO composites were characterized by RM200 confocal Raman spectro microscopy scanned in the range of (100 to 400) cm^{-1} in presence of He and Ni laser beam. The XRD pattern of hybrid composite was studied by Rigaku Rotaflex (RU-200B) X-ray diffractometry, with CuK$_\alpha$ radiation ($\lambda = 1.514$ A°). The surface properties of $Co_3O_4@MnO_2$/NGO were analyzed through field emission scanning electron microscopy (FE-SEM, Hitachi S-4800, and Japan) and filed emission transmission electron microscopy (FE-TEM, JEM-2010F). The elemental analysis of $Co_3O_4@MnO_2$/NGO was examined using X-ray photoelectron spectroscopy (XPS, ESCALAB 250Xi, Thermo Fisher Scientific, and USA). The electrochemical properties of the hybrid composite had evaluated by Bio-Logics Science Instruments SAS Ltd (France). The CV experiment was conducted at ambient temperature prepared $Co_3O_4@MnO_2$/NGO as a working electrode, the reference electrode was Ag/AgCl, and platinum wire was employed as the counter electrode. 6 M KOH served as electrolyte solution. The optimized potential window was in the range between −0.34 and 0.51 V and performed the tests at various scan rates (5 to 100) mV/s and current densities (0.5, 1, and 2) A g^{-1}. The GCD was performed at current densities from (0.5, 1, and 2) A g^{-1}. The electrochemical impedance spectroscopy (EIS) was measured in the frequency range between 0.1 Hz and 100 KHz with a signal amplitude of 500 mV.

Preparation of working electrode (WE).

The WE was prepared by using stoichiometric amounts of $Co_3O_4@MnO_2$/NGO, conductive carbon black, and PVDF in the ratio of 80:15:5 and formed as a slurry using NMP solvent. The slurry thus obtained was weighed (3 mg cm^{-2}) and then coated over the stainless-steel substrate (1 × 1 cm^2 active area). Finally the coated substrate was dried under vacuum at 110 °C for 12 h.

The specific capacitance of $Co_3O_4@MnO_2$/NGO electrode was determined from Eq. (1)[60–62].

$$C = \int \frac{Idt}{m\Delta V} \tag{1}$$

where *I* denote the current, m represents the mass of the active material, *dt* the time interval and ΔV represents the potential difference.

The energy density E (Wh kg^{-1}) and power density P (kW kg^{-1}) was evaluated by means of following expressions 2 & 3,

$$E = \frac{1}{2} \times C(\Delta V^2)/3.6 \tag{2}$$

$$P = E \times 3600/\Delta t \tag{3}$$

In the above equations, ΔV and Δt represents the voltage window and time interval for discharge process respectively[60].

References

1. Falcao, E. H. & Wudl, F. Carbon allotropes: beyond graphite and diamond. *J. Chem. Technol. Biotechnol.* **82**, 524–531 (2007).
2. Georgakilas, V., Perman, J. A., Tucek, J. & Zboril, R. Broad family of carbon nanoallotropes: classification, chemistry, and applications of fullerenes, carbon dots, nanotubes, graphene, nanodiamonds, and combined superstructures. *Chem. Rev.* **115**, 4744–4822 (2015).
3. Iijima, S. Helical microtubules of graphitic carbon. *Nature* **354**, 56 (1991).
4. Lin, Y. *et al.* Holey graphene nanomanufacturing: Structure, composition, and electrochemical properties. *Adv. Funct. Mater.* **25**, 2920–2927 (2015).
5. Li, H., Wu, H., Yuan, S. & Qian, H. Synthesis and characterization of vertically standing MoS$_2$ nanosheets. *Sci. Rep.* **6**, 21171 (2016).
6. Papandrea, B. *et al.* Three-dimensional graphene framework with ultra-high sulfur content for a robust lithium–sulfur battery. *Nano Res.* **9**, 240–248 (2016).
7. Han, X. *et al.* Scalable holey graphene synthesis and dense electrode fabrication toward high-performance ultracapacitors. *ACS Nano* **8**, 8255–8265 (2014).
8. Xu, Y. *et al.* Holey graphene frameworks for highly efficient capacitive energy storage. *Nat. Commun.* **5**, 4554 (2014).
9. Lv, X. *et al.* A hybrid of holey graphene and Mn$_3$O$_4$ and its oxygen reduction reaction performance. *Chem. Commun.* **51**, 3911–3914 (2015).
10. Huang, M., Li, F., Dong, F., Zhang, Y. X. & Zhang, L. L. MnO$_2$-based nanostructures for high-performance supercapacitors. *J. Mater. Chem. A* **3**, 21380–21423 (2015).
11. Zhu, Y. *et al.* Liquid-solid-solution assembly of CoFe$_2$O$_4$/graphene nanocomposite as a high-performance lithium-ion battery anode. *Electrochim. Acta* **215**, 247–252 (2016).
12. Wang, F. *et al.* Co-doped Ni$_3$S$_2$@ CNT arrays anchored on graphite foam with a hierarchical conductive network for high-performance supercapacitors and hydrogen evolution electrodes. *J.Mater. Chem. A* **6**, 10490–10496 (2018).
13. Wang, G., Zhang, L. & Zhang, J. A review of electrode materials for electrochemical supercapacitors. *Chem. Soc. Rev.* **41**, 797–828 (2012).
14. Miller, J. R. & Simon, P. Electrochemical capacitors for energy management. *Science* **321**, 651–652 (2008).
15. Chen, H., Hu, L., Chen, M., Yan, Y. & Wu, L. Nickel–Cobalt Layered Double Hydroxide Nanosheets for High-performance Supercapacitor Electrode Materials. *Adv. Funct. Mater.* **24**, 934–942 (2014).
16. Liu, J. *et al.* Co$_3$O$_4$ Nanowire@ MnO$_2$ Ultrathin Nanosheet Core/Shell Arrays: A New Class of High-Performance Pseudocapacitive Materials. *Adv. Mater.* **23**, 2076–2081 (2011).
17. Zhu, Y. *et al.* PPy@ NiCo$_2$S$_4$ nanosheets anchored on graphite foam with bicontinuous conductive network for high-areal capacitance and high-rate electrodes. *J. Alloys Compd.* **747**, 276–282 (2018).
18. Zhu, S. *et al.* Structural directed growth of ultrathin parallel birnessite on β-MnO$_2$ for high-performance asymmetric supercapacitors. *ACS Nano* **12**, 1033–1042 (2018).

19. Le, Q. J. *et al*. Morphology-controlled MnO₂ modified silicon diatoms for high-performance asymmetric supercapacitors. *J. Mater. Chem. A* **5**, 10856–10865 (2017).

20. Wang, F. *et al*. Construction of vertically aligned PPy nanosheets networks anchored on MnCo₂O₄ nanobelts for high-performance asymmetric supercapacitor. *J. Power Sources* **393**, 169–176 (2018).

21. Lv, X. *et al*. Controllable synthesis of MnO₂ nanostructures anchored on graphite foam with different morphologies for a high-performance asymmetric supercapacitor. *Cryst. Eng. Comm.* **20**, 1690–1697 (2018).

22. Ko, Y. *et al*. Flexible supercapacitor electrodes based on real metal-like cellulose papers. *Nat. Commun.* **8**, 536 (2017).

23. Guan, C. *et al*. Atomic layer deposition of Co₃O₄ on carbon nanotubes/carbon cloth for high-capacitance and ultrastable supercapacitor electrode. *Nanotechnology* **26**, 094001 (2015).

24. Ghosh, D., Giri, S. & Das, C. K. Preparation of CTAB-assisted hexagonal platelet Co (OH)₂/graphene hybrid composite as efficient supercapacitor electrode material. *ACS Sustain. Chem. Eng.* **1**, 1135–1142 (2013).

25. Wei, W., Cui, X., Chen, W. & Ivey, D. G. Manganese oxide-based materials as electrochemical supercapacitor electrodes. *Chem. Soc. Rev.* **40**, 1697–1721 (2011).

26. Yu, P., Zhang, X., Chen, Y., Ma, Y. & Qi, Z. Preparation and pseudo-capacitance of birnessite-type MnO₂ nanostructures via microwave-assisted emulsion method. *Mater. Chem. Phys.* **118**, 303–307 (2009).

27. Wang, X., Yuan, A. & Wang, Y. Supercapacitive behaviors and their temperature dependence of sol–gel synthesized nanostructured manganese dioxide in lithium hydroxide electrolyte. *J. Power Sources* **172**, 1007–1011 (2007).

28. Huang, M. *et al*. Self-assembly of mesoporous nanotubes assembled from interwoven ultrathin birnessite-type MnO₂ nanosheets for asymmetric supercapacitors. *Sci. Rep.* **4**, 3878 (2014).

29. Huang, M. *et al*. Merging of Kirkendall growth and Ostwald ripening: CuO@ MnO₂ core-shell architectures for asymmetric supercapacitors. *Sci. Rep.* **4**, 4518 (2014).

30. Huang, M. *et al*. Layered manganese oxides-decorated and nickel foam-supported carbon nanotubes as advanced binder-free supercapacitor electrodes. *J. Power Sources* **269**, 760–767 (2014).

31. Huang, M. *et al*. Synthesis of Co₃O₄/SnO₂@ MnO₂ core–shell nanostructures for high-performance supercapacitors. *J. Mater. Chem. A* **3**, 12852–12857 (2015).

32. Yuan, C., Zhang, X., Su, L., Gao, B. & Shen, L. Facile synthesis and self-assembly of hierarchical porous NiO nano/micro spherical superstructures for high performance supercapacitors. *J. Mater. Chem.* **19**, 5772–5777 (2009).

33. Yuan, C., Wu, H. B., Xie, Y. & Lou, X. W. D. Mixed transition-metal oxides: design, synthesis, and energy-related applications. *Angew. Chem. Int. Ed.* **53**, 1488–1504 (2014).

34. Wang, H., Casalongue, H. S., Liang, Y. & Dai, H. Ni (OH)₂ nanoplates grown on graphene as advanced electrochemical pseudocapacitor materials. *J. Am. Chem. Soc.* **132**, 7472–7477 (2010).

35. Ren, Z. *et al*. Large-scale synthesis of hybrid metal oxides through metal redox mechanism for high-performance pseudocapacitors. *Sci. Rep.* **6**, 20021 (2016).

36. Lee, S. W., Kim, J., Chen, S., Hammond, P. T. & Shao-Horn, Y. Carbon nanotube/manganese oxide ultrathin film electrodes for electrochemical capacitors. *ACS Nano* **4**, 3889–3896 (2010).

37. Lin, P. *et al*. The nickel oxide/CNT composites with high capacitance for supercapacitor. *J. Electrochem. Soc.* **157**, A818–A823 (2010).

38. Wang, D. W., Li, F., Liu, M., Lu, G. Q. & Cheng, H. M. 3D aperiodic hierarchical porous graphitic carbon material for high-rate electrochemical capacitive energy storage. *Angew. Chem. Int. Ed.* **120**, 379–382 (2008).

39. Ramesh, S., Dhanasekaran, V., Kim, H.-S., Kim, H. S. & Kim, J.-H. Electrochemical performance of MWCNT/GO/NiCo₂O₄ decorated hybrid nanocomposite for supercapacitor electrode materials. *J. Alloys Compds.* **765**, 369–379 (2018).

40. Candelaria, S. L. *et al*. Nanostructured carbon for energy storage and conversion. *Nano Energy* **1**, 195–220 (2012).

41. Wang, Y. & Xia, Y. Recent progress in supercapacitors: from materials design to system construction. *Adv. Mater.* **25**, 5336–5342 (2013).

42. Zhang, L. L. & Zhao, X. Carbon-based materials as supercapacitor electrodes. *Chem. Soc. Rev.* **38**, 2520–2531 (2009).

43. Lu, W., Hartman, R., Qu, L. & Dai, L. Nanocomposite electrodes for high-performance supercapacitors. *J. Phys. Chem. Lett.* **2**, 655–660 (2011).

44. Conway, B. & Pell, W. Double-layer and pseudocapacitance types of electrochemical capacitors and their applications to the development of hybrid devices. *J. Solid State Electrochem.* **7**, 637–644 (2003).

45. Wei, H., Zhu, J., Wu, S., Wei, S. & Guo, Z. Electrochromic polyaniline/graphite oxide nanocomposites with endured electrochemical energy storage. *Polymer* **54**, 1820–1831 (2013).

46. Li, Z. *et al*. High-performance solid-state supercapacitors based on graphene-ZnO hybrid nanocomposites. *Nanoscale Res. Lett.* **8**, 473 (2013).

47. Jang, G. S., Ameen, S., Akhtar, M. S., Kim, E. & Shin, H. S. Electrochemical Investigations of Hydrothermally Synthesized Porous Cobalt Oxide (Co₃O₄) Nanorods: Supercapacitor Application. *Chemistry Select* **2**, 8941–8949 (2017).

48. Numan, A. *et al*. Enhanced electrochemical performance of cobalt oxide nanocube intercalated reduced graphene oxide for supercapacitor application. *RSC Adv.* **6**, 34894–34902 (2016).

49. Liu, H. *et al*. Cauliflower-like Co₃O₄/three-dimensional graphene composite for high performance supercapacitor applications. *J. Nanomater.* **2015**, 11 (2015).

50. Zhang, D. & Zou, W. Decorating reduced graphene oxide with Co₃O₄ hollow spheres and their application in supercapacitor materials. *Curr. Appl. Phys.* **13**, 1796–1800 (2013).

51. He, G. *et al*. Hydrothermal preparation of Co₃O₄@ graphene nanocomposite for supercapacitor with enhanced capacitive performance. *Mater. Lett.* **82**, 61–63 (2012).

52. Park, S. K., Suh, D. H. & Park, H. S. Electrochemical assembly of reduced graphene oxide/manganese dioxide nanocomposites into hierarchical sea urchin-like structures for supercapacitive electrodes. *J. Alloys Compd* **668**, 146–151 (2016).

53. Li, Z. *et al*. Preparation of a two-dimensional flexible MnO₂/graphene thin film and its application in a supercapacitor. *J. Mater. Chem. A* **4**, 10618–10626 (2016).

54. Tao, L. *et al*. Supercapacitor electrode with a homogeneously Co₃O₄-coated multiwalled carbon nanotube for a high capacitance. *Nanoscale Res. Lett.* **10**, 208 (2015).

55. Chen, S., Yang, G., Jia, Y. & Zheng, H. Facile Synthesis of CoWO₄ Nanosheet Arrays Grown on Nickel Foam Substrates for Asymmetric Supercapacitors. *Chem. Electro. Chem* **3**, 1490–1496 (2016).

56. Sharma, V., Singh, I. & Chandra, A. Hollow nanostructures of metal oxides as next generation electrode materials for supercapacitors. *Sci. Rep.* **8**, 1307 (2018).

57. Huang, M. *et al*. Facile synthesis of hierarchical Co₃O₄@ MnO₂ core–shell arrays on Ni foam for asymmetric supercapacitors. *J. Power Sources* **252**, 98–106 (2014).

58. Yan, J. *et al*. Preparation of graphene nanosheet/carbon nanotube/polyaniline composite as electrode material for supercapacitors. *J. Power Sources* **195**, 3041–3045 (2010).

59. Cheng, Q. *et al*. Graphene and nanostructured MnO₂ composite electrodes for supercapacitors. *Carbon* **49**, 2917–2925 (2011).

60. Meher, S. K. & Rao, G. R. Ultralayered Co₃O₄ for high-performance supercapacitor applications. *The J. Phys. Chem. C* **115**, 15646–15654 (2011).

61. Zhang, J. *et al*. δ-MnO₂/holey graphene hybrid fiber for all-solid-state supercapacitor. *J. Mater. Chem. A* **4**, 9088–9096 (2016).

62. Xia, H. *et al*. Hierarchically structured Co₃O₄@ Pt@ MnO₂ nanowire arrays for high-performance supercapacitors. *Sci. Rep.* **3**, 2978 (2013).

Acknowledgements

Author Contributions

S.R., K.K. and H.S.K. planned the project and the experiments. S.R. and K.K. performed the experiments. All authors S.R., H.-S.K., H.S.K., K.K. and J.-H.K. contributed to the data analysis and the discussions leading up to the writing of the manuscript. S.R. and H.S.K. took part in the main discussions that led to the final manuscript; all authors read and finalized the final manuscript.

Additional Information

Competing Interests: The authors declare no competing interests.

Publisher's note: Springer Nature remains neutral with regard to jurisdictional claims in published maps and institutional affiliations.